Lifecycle cost effectiveness of translational and pendulum tuned mass dampers for the seismic mitigation of building structures

Lifecycle cost effectiveness of translational and pendulum tuned mass dampers for the seismic mitigation of building structures

Emiliano Matta

Department of Architecture and Design,
Politecnico di Torino,
C.so Duca degli Abruzzi 24, 10129 Turin, Italy
Email: emiliano.matta@polito.it

Abstract: Lifecycle cost (LCC) analysis is increasingly used by researchers and designers worldwide as a comprehensive and objective tool to evaluate the performance of structural systems, and particularly of dynamic mitigation strategies. Very recently, it has been successfully adopted to assess the cost-effectiveness of linear tuned mass dampers (TMDs) on inelastic building structures under earthquake hazard. In this paper, the analysis is extended to nonlinear TMDs of the pendulum type, where modelling nonlinearities are both geometrical (large angular displacements) and mechanical (collision against the fail-safe bumper). By analysing three benchmark structural models representative of typical office buildings in the Los Angeles area, a comparison between the translational (linear) and the pendulum (nonlinear) alternatives is presented. Results show that the cost-effectiveness of the pendulum TMD is similar to that of the translational TMD in many cases, but may be significantly diminished in the case of short-period structures and small mass ratios, particularly if premature bumping is permitted.

Keywords: lifecycle cost; LCC; cost-effectiveness; tuned mass damper; TMD; seismic retrofitting; geometric nonlinearities; mechanical nonlinearities.

Reference to this paper should be made as follows: Matta, E. (xxxx) 'Lifecycle cost effectiveness of translational and pendulum tuned mass dampers for the seismic mitigation of building structures', *Int. J. Lifecycle Performance Engineering*, Vol. X, No. Y, pp.xxx–xxx.

Biographical notes: Emiliano Matta is an Assistant Professor at the Department of Architecture and Design at Politecnico di Torino, Turin, Italy, where he received his Master's in Civil Engineering in 2002 and his PhD in Structural Engineering in 2006. He is the author of more than 50 papers on top rank international journals and conference proceedings, mostly in the fields of structural dynamics and seismic engineering, structural health monitoring and vibration control. He has a long-term experience as a professional and consultant engineer, mainly on the themes of structural design, seismic and forensic engineering.

1 Introduction

Tuned mass dampers (TMDs) are one of the most common dynamic control systems employed in civil engineering (Spencer and Nagarajaiah, 2003). Mainly installed on flexible structures exposed to quasi-stationary dynamic loads, they are less frequently used to improve the response of building structures to earthquakes, their seismic effectiveness still being a debated issue, particularly in the case of nonlinear structures (Villaverde and Koyama, 1993; Sadek et al., 1997; Soto-Brito and Ruiz, 1999; Lukkunaprasit and Wanitkorkul, 2001; Pinkaew et al., 2003; Wong, 2008). In this respect, the current literature tends to recognise the satisfactory performance of TMDs in controlling inelastic structures under low-to-moderate earthquakes (weak nonlinearities) but also their performance degradation in the event of severe ground motions (strong nonlinearities).

Conventional performance criteria based on the reduction of some representative engineering demand parameter (EDP), such as peak displacement or peak acceleration, are inadequate to concisely represent such trade-off between intensity and effectiveness, because they cannot weigh the relative economic importance of different hazard levels. Alternatively, this can be achieved by applying to the coupled structure-TMD system a lifecycle cost (LCC) estimation, capable to reflect, through a probabilistic treatment of the seismic hazard, the relative impact of different earthquake intensities on the expected cost of future seismic damages and losses. Integrated with the estimation of the initial TMD investment cost, LCC analysis provides a rational and objective measure of TMD cost-effectiveness, already expressed in monetary units and applicable to both new and existing structures. The sum of the investment cost and the lifetime costs determines the total LCC of the overall system, whose minimisation can be taken as the primary design objective.

In recent years, LCC analysis has been increasingly applied by researchers and designers worldwide to the assessment and the optimisation of seismic engineering systems (e.g., Sanchez-Silva and Rackwitz, 2004; Kappos and Dimitrakopoulos, 2008) and particularly of vibroprotective devices (Taflanidis and Beck, 2009; Shin and Singh, 2014; Hahm et al., 2013). LCC principles have also been applied to TMDs, typically assuming a linear behaviour of the main structure (Huang et al., 2011; Wang et al., 2015; Ruiz et al., 2016). Only very few studies have modelled the main structure as an inelastic system, and none of them has described the TMD too as a nonlinear device (Taflanidis et al., 2009; Lee et al., 2012; Matta, 2017).

In this paper, LCC analysis is extended to nonlinear TMDs of the pendulum type (PTMD). The nonlinearities accounted for in the TMD model are both geometrical, related to large-amplitude pendular oscillations, and mechanical, due to the TMD colliding against a fail-safe bumper. The LCC performance of the PTMD is compared with that of a classical linear TMD of the translational type (TTMD), assuming different mass ratios and, for the PTMD, different bumper clearances. For the two TMD types, a TMD retrofit intervention is simulated on different models of existing buildings, simulated as inelastic structures under earthquake loading. The three SAC steel project benchmark buildings, representative of typical steel moment-resisting frame (MRF) office buildings in the Los Angeles area, are in turn used as the main structure (Gupta and Krawinkler, 1999).

2 The structural model

In this paper, three-dimensional (3D) inelastic MRF building structures equipped with a single TMD are simulated under bidirectional ground motion input. For simplicity, because of the symmetry of the examined structural configuration (which prevents building rotations around the vertical axis), analysis is conducted separately along each horizontal direction, on the basis of planar (2D) finite element (FE) models. Material nonlinearity is concentrated in bilinear hardening-type inelastic hinges located at the ends of columns and beams. The TMD is modelled as a SDOF appendage attached to the top storey and tuned to the fundamental structural mode (target mode). The appendage is either a linear mass-spring-dashpot system (TTMD) or a viscously-damped nonlinear pendular mass complemented with a nonlinear fail-safe bumper (PTMD). In this latter case, the geometric nonlinear coupling of the pendulum response components in the two horizontal directions is neglected for simplicity.

Figure 1 Schematics of a TTMD (a) and of a PTMD (b) on the top storey

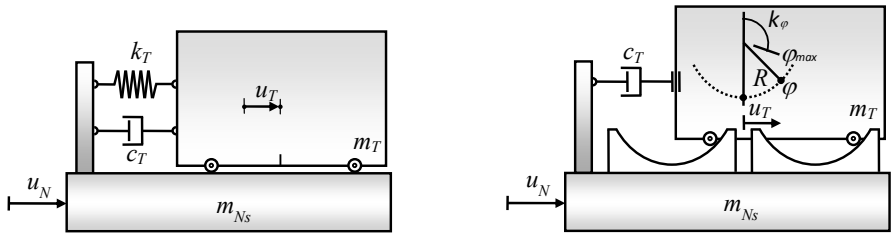

(a) (b)

The equations of motion for an NS-storey inelastic MRF planar structure coupled with a TMD and subjected to ground accelerations can be written as follows, respectively for the main structure and for the TMD:

$$\mathbf{M}\ddot{\mathbf{u}} + \mathbf{C}\dot{\mathbf{u}} + \mathbf{f}_r + \mathbf{f}_{P-\Delta} = -\mathbf{M}\mathbf{t}_g\ddot{u}_g + \mathbf{t}_p p_T \tag{1}$$

$$m_T\left(\ddot{u}_g + \ddot{u}_{Ns} + \ddot{u}_T\right) = -p_T \tag{2}$$

where

$$\mathbf{f}_{P-\Delta} = -\mathbf{P}\boldsymbol{\theta} = -\mathbf{P}\mathbf{T}\mathbf{u} = \mathbf{K}_{P-\Delta}\mathbf{u} \tag{3}$$

And $\mathbf{u} = [u_1\ u_2\ \ldots\ u_{Ns}]^T$ and $\dot{\mathbf{u}}$ are the vectors of horizontal structural displacements and velocities relative to the ground; **M** and **C** are the structural mass and damping matrices; $\mathbf{f}_r$ is the vector of lateral restoring forces; $\ddot{u}_g$ is the ground acceleration input; u_T is the horizontal displacement of the TMD relative to the top storey (stroke); m_T is the mass of the TMD; p_T is the structure-TMD interaction force; $t_g = [1\ 1\ \ldots\ 1]^T$ and $t_p = [0\ \ldots\ 0\ 1]^T$ are the topological vectors for, respectively, the ground acceleration and the interaction force; $\mathbf{f}_{P-\Delta}$ is the vector of P-delta forces accounting for second-order effects; **P** is the matrix of P-delta cumulative gravity load; $\boldsymbol{\theta} = \left[\theta_1\ \theta_2\ \ldots\ \theta_{Ns}\right]^T$ is the vector of inter-storey drift ratios; **T** is a rotation matrix, transforming the displacement vector **u** into the inter-

storey drift ratio vector $\boldsymbol{\theta}$; $\mathbf{K}_{P\text{–}\Delta} = \text{–}\mathbf{PT}$ is the geometric stiffness matrix accounting for P-delta effects.

The expression of the interaction force p_T in equation (2) depends on the chosen TMD type. In the case of the TTMD [Figure 1(a)], denoting by c_T and k_T respectively the TMD damping and stiffness coefficients, the interaction force is expressed by:

$$p_T = c_T \dot{u}_T + k_T u_T \tag{4}$$

In the case of the PTMD [Figure 1(b)], denoting by R and φ the pendulum length and the pendulum angular displacement, by k_φ and $\varphi_{\max}$ the rotational stiffness and the angular clearance of the associated fail-safe bumper (modelled as a non-dissipative gap element), and by g the gravity acceleration, the interaction force is expressed by:

$$p_T = m_T R\ddot{\varphi}\sin\varphi\tan\varphi + c_T R\cos\varphi\dot{\varphi} + m_T g\tan\varphi + m_T R\sin\varphi\dot{\varphi}^2 + \chi(\varphi)/\cos\varphi \tag{5}$$

where $\chi(\varphi) = \rho m_T g(|\varphi| - \varphi_{\max})\text{sgn}\ \varphi\ \text{step}(|\varphi| - \varphi_{\max})$ is the tangential force transmitted by the PTMD to the bumper and $\rho = (k_\varphi/R)/(m_T g)$ is the ratio between the equivalent bumper stiffness and the equivalent pendulum stiffness at small angular deflections (Matta and De Stefano, 2009).

If the structure responds in the linear elastic range, the restoring force vector can be expressed as $\mathbf{f}_r = \mathbf{K}_e\mathbf{u}$ and equation (1) becomes:

$$\mathbf{M}\ddot{\mathbf{u}} + \mathbf{C}\dot{\mathbf{u}} + \mathbf{K}\mathbf{u} = -\mathbf{M}\mathbf{t}_g\ddot{u}_g + \mathbf{t}_p p_T \tag{6}$$

where $\mathbf{K}_e$ is the first-order elastic stiffness matrix of the structure and $\mathbf{K} = \mathbf{K}_e + \mathbf{K}_{P\text{–}\Delta}$ is the total stiffness matrix of the structure including second-order effects. Equation (6) is then certainly linear for a TTMD, and can be linearised for a PTMD by making the further assumption of small-angular displacements. If equation (6) is linear, classical input-output transfer functions (TFs) can be computed for the coupled structure-TMD system, which turn useful in selecting the appropriate TMD parameters for design, as it will be explained in the sequel.

3 The LCC analysis procedure

3.1 Generalities

Several LCC analysis methods have been recently developed for estimating the lifetime cost of building structures in an earthquake mitigation perspective (Taflanidis and Beck, 2009). The approach introduced by Wen and Kang (2001) and later improved by Lagaros and co-authors (e.g., Fragiadakis and Lagaros, 2011) is here adopted. The approach makes damage and therefore lifetime cost depends on one or more seismic EDPs, computed at multiple intensity levels through dynamic nonlinear analyses. Based on the so-called multiple-stripe dynamic analysis (MSDA) method, many groups of nonlinear dynamic analyses (stripes) are performed at increasing intensities, each corresponding to a predetermined exceedance probability in a given time period, according to the hazard curve of the site. In this way, the relation is obtained between the seismic intensity and the corresponding structural response, expressed by a significant EDP. Selecting the appropriate EDP is a fundamental step in MSDA (Ghobarah et al., 1999). For MRF buildings there is wide consensus on the inter-storey drift ratio θ as the best EDP based

on maximum deformation (Gupta and Krawinkler, 1999). Established relations exist between θ and performance-oriented descriptions, such as immediate occupancy, life safety and collapse prevention (FEMA-273, 1997), and between θ and damage, both for reinforced concrete and steel frame structures.

In this paper, MSDA is applied to 2D structural models representative of in-plan symmetrical spatial buildings under bidirectional ground motions. MSDA is conducted by considering $N_L = 7$ intensity levels, each described by a set of $N_R = 10$ two-component spectrum-compatible records. θ is chosen as the EDP and the relation between θ and damage is taken as proposed by Wen and Kang (2001), distinguishing among the $N_D = 7$ damage states defined in Table 1 (columns 1 and 2). For every storey, the EDP representing a given intensity, denoted as the set-EDP, is computed:

1 first, by evaluating the record-EDP as the largest EDP between the two components of each record

2 then, by computing the set-EDP as the mean of all record-EDPs in that set.

Table 1 Damage state parameters for cost evaluation

Damage state	*EDP range (%)*	*Mean damage index (%)*	*Downtime index (%)*	*Minor injury rate*	*Serious injury rate*	*Death rate*
1-None	$0.0 \le \theta < 0.2$	0	0	0	0	0
2-Slight	$0.2 \le \theta < 0.5$	0.5	0.9	$3.0 \cdot 10^{-5}$	$4.0 \cdot 10^{-6}$	$1.0 \cdot 10^{-6}$
3-Light	$0.5 \le \theta < 0.7$	5	3.33	$3.0 \cdot 10^{-4}$	$4.0 \cdot 10^{-5}$	$1.0 \cdot 10^{-5}$
4-Moderate	$0.7 \le \theta < 1.5$	20	12.4	$3.0 \cdot 10^{-3}$	$4.0 \cdot 10^{-4}$	$1.0 \cdot 10^{-4}$
5-Heavy	$1.5 \le \theta < 2.5$	45	34.8	$3.0 \cdot 10^{-2}$	$4.0 \cdot 10^{-3}$	$1.0 \cdot 10^{-3}$
6-Major	$2.5 \le \theta < 5.0$	80	65.4	$3.0 \cdot 10^{-1}$	$4.0 \cdot 10^{-2}$	$1.0 \cdot 10^{-2}$
7-Destroyed	$5.0 \le \theta$	100	100	$4.0 \cdot 10^{-1}$	$4.0 \cdot 10^{-1}$	$2.0 \cdot 10^{-1}$

Source: Mitropoulou et al. (2011)

3.2 LCC model

The expected LCC of the coupled structure-TMD system over a time period t (the design life of a new structure or the remaining life of an existing structure) can be expressed by:

$$C_{TOT} = -C_{IN,S} + C_{DS,S} + C_{IN,T} + C_{DS,T} \tag{7}$$

where $C_{IN,S}$ and $C_{IN,T}$ are the initial costs of the structure and the TMD, and $C_{DS,S}$ and $C_{DS,T}$ are the present value of the expected costs of future seismic damages suffered by, respectively, the structure and the TMD during the future lifetime period t. The building initial cost $C_{IN,S}$ refers to the material and labour costs for constructing a new building or for retrofitting an existing one. The TMD initial cost $C_{IN,T}$ refers to the costs for designing and constructing the TMD. The building damage cost $C_{DS,S}$ refers to the cost of structural and non-structural repair, loss of contents, rental and income losses, injury recovery and human fatality. The TMD damage cost $C_{DS,T}$ refers to the loss of the TMD in case of building collapse.

Subtracting $C_{IN,S}$ from C_{TOT}, the 'controllable' lifecycle cost C is obtained as:

$$C = C_{TOT} - C_{IN,S} = C_{DS,S} + C_{IN,T} + C_{DS,T} \tag{8}$$

Which represents the part of LCC which can be reduced through retrofitting. Denoting as C_{unc} the value of C corresponding to the uncontrolled configuration (i.e., computed according to equation (8) for the structure with no TMD), the cost savings produced by the TMD are expressed by $C_{save} = C_{unc} - C$ which, normalised to C_{unc}, result in the TMD cost-effectiveness CE as follows:

$$CE = C_{save} / C_{unc} = 1 - C / C_{unc} \tag{9}$$

3.2.1 Building damage cost

In equation (8), $C_{DS,S}$ is caused by N_D possible damage states. According to Mitropoulou et al. (2011), the cost of the i^{th} damage state can be computed as:

$$C^i_{DS,S} = C^i_{dam} + C^i_{con} + C^i_{ren} + C^i_{inc} + C^i_{inj} + C^i_{fat} \tag{10}$$

where C^i_{dam} is the damage repair cost, C^i_{con} is the loss of contents cost, C^i_{ren} is the loss of rental cost, C^i_{inc} is the loss of income cost, C^i_{inj} is the injury cost and C^i_{fat} is the human fatality cost. Each damage state cost is computed by applying the formulas described in Table 2 with the damage state parameters reported in Table 1 (columns 3 to 7) and with the unit costs reported in Table 3.

Table 2 Formulas for computing the damage state costs

Cost category	*Calculation formula*
Damage repair	Replacement cost × floor area × mean damage index
Loss of content	Unit content cost × floor area × mean damage index
Income	Income rate × gross leasable area[(ii)] × disruption period[(iii)] × downtime index
Minor injury	Minor injury cost per person × floor area × occupancy rate[(i)] × minor injury rate
Serious injury	Serious injury cost per person × floor area × occupancy rate[(i)] × serious injury rate
Fatality	Death cost per person × floor area × occupancy rate[(i)] × death rate

Note: [(i)]Occupancy rate: 2 persons/100 m^2; [(ii)]gross leasable area: 90% of the total floor area; [(iii)]disruption period: 6 months.

Source: Fragiadakis and Lagaros (2011)

Assuming a Poisson model of earthquake occurrences, $C_{DS,S}$ can be evaluated as:

$$C_{DS,S} = \nu \left(\frac{1 - e^{-\lambda t}}{\lambda} \right) \sum_{i=1}^{N_D} C^i_{DS,S} P^i_o \tag{11}$$

where P^i_o is the occurrence probability of the i^{th} damage state given the occurrence of a significant earthquake; ν is the mean occurrence frequency of significant earthquakes; and λ is the momentary discount rate. Denoting the ratio in parentheses as the actualised lifetime period t_a, equation (11) can be rewritten as:

$$C_{DS,S} = t_a \sum_{i=1}^{N_D} C_{DS,S}^i \phi_o^i \tag{12}$$

where $\phi_o^i = \nu P_o^i$ is the mean occurrence frequency of the i^{th} damage state. Denoting as θ^i the lower bound for the i^{th} damage state, ϕ_o^i in equation (12) is obtained as:

$$\phi_o^i = \phi_e^i - \phi_e^{i+1} \tag{13}$$

where ϕ_e^i is the mean exceedance frequency of θ^i and can be expressed by a relation of the form:

$$\phi_e^i = f(\theta^i) \tag{14}$$

Table 3 Unit costs for each cost category

Cost category	*Unit costs*
Replacement cost	1,500 €/m^2
Unit content cost	500 €/m^2
Income rate	3,200 €/year/m^2
Minor injury cost per person	2,000 €/person
Serious injury cost per person	$2 \cdot 10^4$ €/person
Death cost per person	$2.8 \cdot 10^6$ €/person

Source: Fragiadakis and Lagaros (2011)

Such relation is deduced through fitting a properly shaped function f to N_L known $\phi_e^j - \theta^j$ pairs, each pair corresponding to a specific intensity level characterised by a known probability of exceedance $P_{e/\tau}^j$ in a given time period τ. For each pair, i.e., for each of the N_L intensity levels, the drift ratio θ^j is computed through nonlinear dynamic analyses as the set-EPS (as explained in Section 2.3.1), while the mean frequency of exceedance of θ^j, denoted as ϕ_e^j, is derived, according to Poisson's law, as:

$$\phi_e^j = -\frac{1}{\tau} \ln\left(1 - P_{e/\tau}^j\right) \tag{15}$$

The fitting function *f* in equation (14) is here assumed as proposed in Matta (2017).

3.2.2 TMD initial and damage costs

Few TMD cost models are available in the literature to derive the TMD initial cost $C_{IN,T}$ and the TMD damage cost CDS,T required in equation (8) (Wang et al., 2015; Ruiz et al., 2016).

A proportional dependence of the TMD initial cost on the TMD mass is adopted in this paper, expressed by:

$$C_{IN,T} = c_U \cdot m_T \tag{16}$$

where the unit cost c_U is here taken as 2,500 €/ton (Matta, 2017). It might be argued that equation (16) does not account for the dependence of the TMD initial cost on the TMD stroke demand, which however plays an important role in TMD design. This is because of the unavailability, in the literature, of explicit relations between the TMD initial cost and the TMD stroke demand.

On the other hand, assuming the TMD effective and undamaged as long as the building avoids collapse, the TMD damage cost $C_{DS,T}$ can be evaluated as follows:

$$C_{DS,T} = t_a C_{IN,T} \phi_0^{N_D} \tag{17}$$

Based on equations (16) and (17), the TMD LCC is finally given by:

$$C_T = C_{IN,T} + C_{DS,T} = \left(1 + t_a \phi_0^{N_D}\right) C_{IN,T} \text{ A} \tag{18}$$

where the product $t_a \phi_0^{N_D}$ gives the collapse probability in the period t_a and is much smaller than unity, so that $C_T \approx C_{IN,T}$.

4 The TMD design procedure

Several methods have been proposed for the optimal design of TMDs in seismic applications. One of the most successful and common approaches continues to be the classical H_∞ design method, consisting in the minimisation of the H_∞ norm of a significant input-output TF of the linearised structure-TMD coupled model (Pinkaew et al., 2003).

The H_∞ design is therefore adopted in the present paper, where the TF is chosen as the one from the ground acceleration to the maximum inter-storey drift ratio, computed according to the linearised model expressed by equation (6). More specifically, denoting by m_S the total mass of the uncontrolled structure, by ω_S and ζ_S the circular frequency and the damping ratio of the structural target mode, and by ω_T and ζ_T the circular frequency and the damping ratio of the TMD, design is conducted as follows: first, the mass ratio $\mu = m_T / m_S$ is arbitrarily assigned, based on cost-benefit expectations; then, the optimal frequency ratio $r = \omega_T / \omega_S$ and damping ratio ζ_T are numerically determined which make the H_∞ norm of the selected TF minimum.

The said method is here applied to the design of both the linear TTMD and the nonlinear PTMD. Obviously, the TMD circular frequency is computed as $\omega_T = \sqrt{k_T / m_T}$ for the TTMD and as $\omega_T = \sqrt{g/R}$ for the PTMD, while the damping ratio is computed in both cases as $\zeta_T = c_T / (2\ \omega_T\ m_T)$. Additionally, the PTMD has two other free design parameters to be assigned, i.e., the stiffness k_φ and the angular clearance $\varphi_{\max}$ of the fail-safe bumper. The bumping stiffness is here assigned through the stiffness ratio $\rho = \left(k_\omega / R\right) / \left(m_T g\right) = \omega_\varphi^2 / \omega_T^2$, here assumed equal to 400 in order to make the bumping frequency ω_φ 20 times larger than the TMD frequency ω_T, so as to represent a relatively rigid boundary. On the other hand, two values of $\varphi_{\max}$ are here adopted for comparison, respectively equal to 60° and to 30°, resulting in two alternative PTMD options here denoted as PTMD-60 and PTMD-30.

5 The case studies: problem setting

In this paper, the TMD design and evaluation procedure explained above is used to simulate the seismic retrofit of three inelastic structures, representative of existing standard office buildings in highly seismic regions. These structures are the 3, 9 and 20-storey steel MRF buildings designed for Los Angeles (LA, California) by Brandow & Johnston Associates in the framework of the SAC Phase II Steel Project (Gupta and Krawinkler, 1999), and later adopted as the three benchmark problems for seismically excited nonlinear buildings (Ohtori et al., 2004). The three structures, here denoted as B03, B09 and B20, respectively represent standard low, medium and high-rise office buildings designed according to pre-Northridge standards (UBC 1994). Each building has a lateral load-resisting system consisting of four identical perimeter steel MRFs (two in each horizontal direction), and interior bays with simple framing and composite floors. Due to the in-plan symmetry of the spatial structure, a unique planar (2D) FE model is adopted to simulate the building response in both directions. For each building, the FE model is a slight variant of the original model developed in MATLAB by Ohtori et al. (2004) and publicly shared within the benchmark control project for seismically excited nonlinear buildings. The original model represents a steel MRF structure with no strength and stiffness degradation. Columns and beams are modelled as linear beam-type elements with inelastic hinges at their ends. The inelastic hinges are characterised by a bilinear moment-rotation law with a 3% strain-hardening. A Rayleigh damping is assumed with 2% damping ratio in the first two modes. With respect to the original model, the one adopted herein is augmented to account for second-order effects and to incorporate the TMD. Coherently with the general scheme presented in Section 1, this is done by including in equation (1) the P-delta force vector $\mathbf{f}_{P-\Delta}$ and the structure-TMD interaction force p_T, in addition to the lateral restoring force vector $\mathbf{f}_r$ already provided by the original model. Figure 2 shows the schematics of the three planar frames. Table 4 reports their main characteristics.

Figure 2 Schematics of the three buildings' elevations

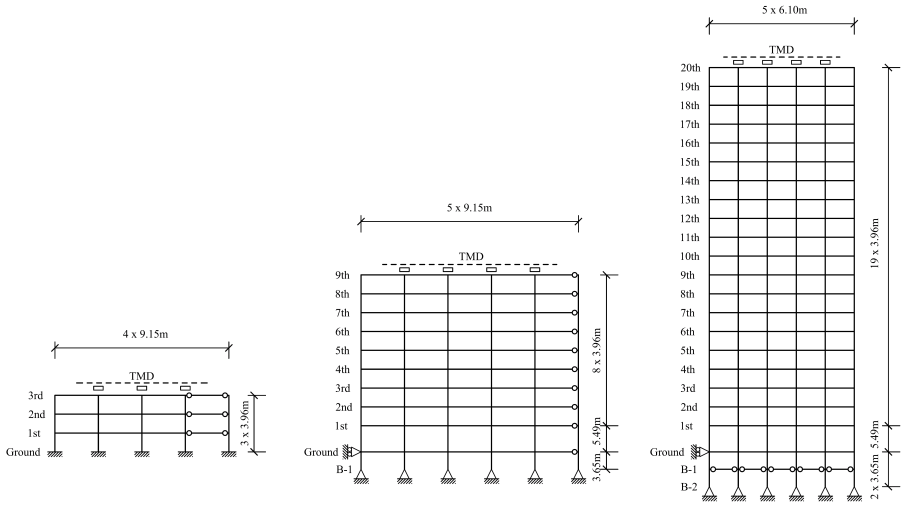

In the simulation, three types of TMDs are compared for each building: the TTMD, the PTMD-60 (φ_{max} = 60°) and the PTMD-30 (φ_{max} = 30°). Each option is simulated while assuming for the mass ratio two alternative values, respectively μ = 1% and μ = 10%. In all cases, the TMD parameters are derived as explained in Section 4.

For both the uncontrolled and the controlled structures, nonlinear dynamic analyses are conducted based on the MSDA approach described in Section 3. N_L = 7 levels of increasing seismic intensity are considered, defined in Table 5. Each intensity is described by a set of 20 time histories, i.e., by N_R = 10 seismic records with two orthogonal components each. Every set is defined in accordance with the seismic hazard at the site. Sets 5 to 7 are taken from the SAC steel research project (Somerville et al., 1997), and consist of recorded and simulated ground motions scaled so that, on average, their spectral ordinates fit with a least square error the values mapped by the United States Geological Survey (USGS). Sets 1 to 4 are obtained through scaling all records in set 5 so as to ensure the compatibility with the USGS spectral values. For each record, the 2D models are separately simulated under both horizontal components, and the overall spatial response of the 3D building is finally reconstructed by virtue of its in-plan symmetry.

Table 4 Main features of the three buildings

Building characteristics		*B03*	*B09*	*B20*
Dimensions (m)	Length	36.58	45.73	30.48
	Width	54.87	45.73	36.58
	Height	11.89	37.19	80.77
Masses (10^5 kg)	Ground level	-	9.65	5.32
	First level	9.57	10.1	5.63
	Top level	10.4	10.7	5.84
	Other levels	9.57	9.89	5.52
Frequencies (Hz)	Mode 1	0.977	0.432	0.252
	Mode 2	3.031	1.154	0.733
	Mode 3	5.792	2.010	1.270

Table 5 The N_L = 7 intensity levels

Set j	*1*	*2*	*3*	*4*	*5*	*6*	*7*
τ (years)	2	5	10	30	50	50	50
$P^j_{e/\tau}$ (%)	50	50	50	50	50	10	2
ϕ_e^j (n/year)	$3.466 \cdot 10^{-1}$	$1.386 \cdot 10^{-1}$	$6.931 \cdot 10^{-2}$	$2.310 \cdot 10^{-2}$	$1.386 \cdot 10^{-2}$	$2.107 \cdot 10^{-3}$	$4.041 \cdot 10^{-4}$

Based on the said nonlinear analyses, the TMD performance is evaluated by comparing the response of the buildings respectively in the uncontrolled and the controlled cases. Comparison is made both in terms of conventional performance indices and in terms of LCC-effectiveness.

On the one hand, five performance indices are considered at each seismic intensity. For each set of records, indices J_1 to J_4 are defined as the ratio of the controlled to the uncontrolled mean value of a given response quantity. Therefore, the smaller the index the better the performance. The corresponding four response quantities are respectively

defined as follows (where 'maximum' denotes the largest value along the building height and 'peak' denotes the largest absolute value along the time axis): the maximum peak inter-storey drift ratio (J_1); the maximum peak absolute acceleration (J_2); the peak base shear force (J_3); the total energy dissipated by the structure in the inelastic hinges at the members ends (J_4). Index J_5, finally, is defined as the mean value of the peak TMD horizontal stroke, expressed in metres.

On the other hand, LCC analysis is conducted according to Section 3, assuming a 50-year lifetime period t and a 2%/year discount rate λ, i.e., an actualised time period $t_a = 31.6$ years.

The main steps of the aforesaid design and evaluation process are described in the remaining of this paper.

6 The case studies: TMD design and evaluation

For the three buildings and the two mass ratios, Table 6 summarises the main TMD parameters obtained by applying the design procedure described in Section 4. The first four lines refer to both the TTMD and the PTMD, while the last two lines refer to the PTMD only. Expectedly, the TMD frequency f_T progressively decreases as the building becomes more flexible (from B03 to B20) and as the mass ratio increases, so that the PTMD pendulum radius R increases from 0.28 m (B03 with $\mu = 1\%$) to 6.39 m (B20 with $\mu = 10\%$).

Table 6 The main TMD parameters

TMD parameters	*B03*		*B09*		*B20*	
	$\mu = 1\%$	$\mu = 10\%$	$\mu = 1\%$	$\mu = 10\%$	$\mu = 1\%$	$\mu = 10\%$
m_T (10^5 kg)	0.295	2.949	0.900	9.001	1.108	11.08
r (–)	0.967	0.802	0.966	0.778	0.965	0.783
ζ_T (–)	0.085	0.243	0.092	0.267	0.094	0.265
f_T (Hz)	0.945	0.783	0.417	0.336	0.243	0.197
R (m)	0.278	0.405	1.430	2.203	4.202	6.386
φ_{max} (°)	60/30	60/30	60/30	60/30	60/30	60/30

Figures 3 and 4 exemplify the time response of building B03 with or without a TMD having $\mu = 1\%$ (alternatively a TTMD, a PTMD-60 or a PTMD-30). The response is computed under a typical seismic record belonging to, respectively, the seismic set 2, corresponding to a 50% probability of exceedance in 5 years (Figure 3) and to the seismic set 7, corresponding to a 2% probability of exceedance in 50 years (Figure 4). Both figures report in particular: the inter-storey drift ratio at the storey where its peak is maximum (θ_3 in Figure 3 and θ_2 in Figure 4); the absolute acceleration at the storey where its peak is maximum (A_3 in Figure 3 and A_1 in Figure 4); the shear force at the base of the building (V_b); the TMD stroke (u_T); the structure-TMD interaction force (p_T); and the TMD constitutive relation ($u_T - p_T$). It can be observed that under a minor seismic level (Figure 3) the three TMDs give nearly indistinguishable results (the red and the blue lines corresponding to the TTMD and the PTMD-60 are completely hidden by the green lines corresponding to the PTMD-30), because nonlinearities are limited and the fail-safe

bumper is not even activated for the PTMD; they also achieve a visible response reduction with respect to the uncontrolled case. On the contrary, under a severe seismic level (Figure 4) the TMD does not produce any advantage over the uncontrolled structure, and the three TMD options show different responses, especially in terms of u_T and p_T because of the activation of the bumper, which occurs earlier for the PTMD-30 and later for the PTMD-60.

Figure 3 Uncontrolled and controlled time response of building B03 to one of the records belonging to the seismic set $j = 2$ (50% probability of exceedance in 5 years), for $\mu = 1\%$ (see online version for colours)

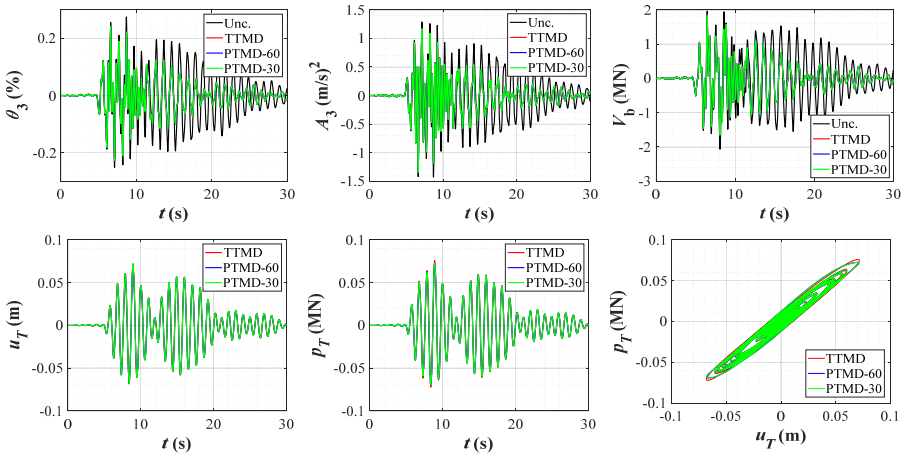

Figure 4 Uncontrolled and controlled time response of building B03 to one of the records belonging to the seismic set $j = 7$ (2% probability of exceedance in 50 years), for $\mu = 1\%$ (see online version for colours)

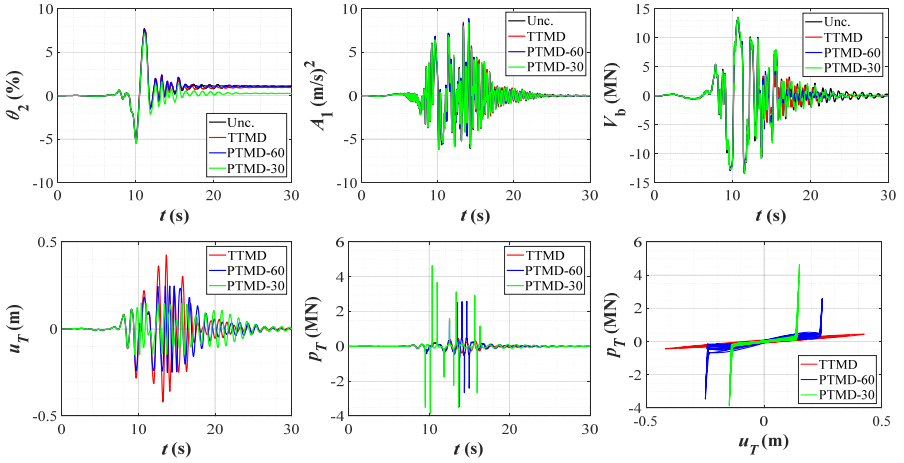

Table 7 Building B03 with μ = 1% – performance indices for the three TMD types

Set j	*TTMD*					*PTMD-60*					*PTMD-30*				
	J_1	J_2	J_3	J_4	J_5	J_1	J_2	J_3	J_4	J_5	J_1	J_2	J_3	J_4	J_5
1	0.84	0.93	0.85	0.00	0.02	0.84	0.93	0.85	0.00	0.02	0.84	0.93	0.85	0.00	0.02
2	0.84	0.93	0.85	0.00	0.09	0.84	0.93	0.85	0.00	0.09	0.84	0.93	0.85	0.00	0.08
3	0.84	0.94	0.86	0.71	0.19	0.84	0.94	0.86	0.72	0.17	0.87	0.94	0.89	0.78	0.13
4	0.91	0.97	0.94	0.55	0.39	0.94	0.98	0.96	0.70	0.23	0.98	0.99	1.01	0.86	0.15
5	0.92	0.98	0.96	0.57	0.46	0.95	0.99	0.98	0.77	0.24	0.96	1.00	1.02	0.91	0.15
6	0.98	1.01	1.00	0.89	0.52	0.99	1.00	1.00	0.96	0.25	1.02	0.99	1.03	1.00	0.15
7	1.02	0.99	1.00	0.98	0.52	1.04	1.00	1.00	1.00	0.25	1.02	1.00	1.07	1.01	0.15

Table 8 Building B03 with μ = 10% – performance indices for the three TMD types

Set j	*TTMD*					*PTMD-60*					*PTMD-30*				
	J_1	J_2	J_3	J_4	J_5	J_1	J_2	J_3	J_4	J_5	J_1	J_2	J_3	J_4	J_5
1	0.67	0.79	0.63	0.00	0.01	0.68	0.79	0.63	0.00	0.01	0.68	0.79	0.63	0.00	0.01
2	0.67	0.79	0.63	0.00	0.03	0.68	0.79	0.63	0.00	0.03	0.68	0.79	0.63	0.00	0.03
3	0.68	0.81	0.65	0.00	0.06	0.68	0.82	0.65	0.00	0.06	0.68	0.82	0.65	0.00	0.06
4	0.76	0.88	0.75	0.34	0.13	0.76	0.88	0.75	0.34	0.13	0.76	1.08	0.78	0.33	0.13
5	0.79	0.91	0.82	0.33	0.16	0.79	0.91	0.83	0.34	0.16	0.79	1.19	0.85	0.32	0.16
6	1.00	0.99	0.97	0.62	0.27	1.00	0.99	0.98	0.64	0.26	1.08	1.62	1.20	0.75	0.21
7	1.09	1.01	0.98	0.92	0.32	1.10	1.00	0.99	0.92	0.29	1.14	1.62	1.36	1.00	0.21

Table 9 Building B09 with μ = 1% – performance indices for the three TMD types

Set j	*TTMD*					*PTMD-60*					*PTMD-30*				
	J_1	J_2	J_3	J_4	J_5	J_1	J_2	J_3	J_4	J_5	J_1	J_2	J_3	J_4	J_5
1	0.93	0.98	0.89	0.01	0.03	0.93	0.98	0.89	0.01	0.03	0.93	0.98	0.89	0.01	0.03
2	0.93	0.98	0.89	0.01	0.13	0.93	0.98	0.89	0.01	0.13	0.93	0.98	0.89	0.01	0.13
3	0.93	0.98	0.89	0.58	0.29	0.93	0.98	0.89	0.58	0.29	0.93	0.98	0.89	0.58	0.29
4	0.93	0.99	0.90	0.87	0.73	0.93	0.99	0.90	0.87	0.70	0.94	1.02	0.90	0.87	0.61
5	0.94	0.99	0.95	0.76	0.91	0.95	0.99	0.95	0.78	0.84	0.96	1.03	0.96	0.77	0.67
6	0.98	1.00	0.99	0.84	1.46	0.98	1.00	0.99	0.86	1.19	0.98	1.00	0.99	0.93	0.74
7	0.98	1.01	1.00	0.95	1.48	0.98	1.00	1.00	0.96	1.20	1.00	1.16	1.00	0.99	0.76

Table 10 Building B09 with μ = 10% – performance indices for the three TMD types

Set j	*TTMD*					*PTMD-60*					*PTMD-30*				
	J_1	J_2	J_3	J_4	J_5	J_1	J_2	J_3	J_4	J_5	J_1	J_2	J_3	J_4	J_5
1	0.78	0.85	0.68	0.00	0.01	0.78	0.85	0.68	0.00	0.01	0.78	0.85	0.68	0.00	0.01
2	0.78	0.85	0.68	0.00	0.05	0.78	0.85	0.68	0.00	0.05	0.78	0.85	0.68	0.00	0.05
3	0.78	0.85	0.68	0.00	0.11	0.78	0.85	0.68	0.00	0.11	0.78	0.85	0.68	0.00	0.11
4	0.77	0.86	0.70	0.61	0.27	0.77	0.86	0.70	0.61	0.27	0.77	0.86	0.70	0.61	0.27
5	0.80	0.88	0.78	0.45	0.35	0.80	0.88	0.78	0.45	0.35	0.80	0.88	0.78	0.45	0.35
6	0.85	1.02	0.95	0.49	0.71	0.85	1.01	0.95	0.50	0.70	0.85	1.01	0.95	0.50	0.70
7	0.88	1.02	0.98	0.79	0.84	0.88	1.00	0.98	0.80	0.82	0.88	1.00	0.98	0.80	0.82

Table 11 Building B20 with μ = 1% – performance indices for the three TMD types

Set j	*TTMD*					*PTMD-60*					*PTMD-30*				
	J_1	J_2	J_3	J_4	J_5	J_1	J_2	J_3	J_4	J_5	J_1	J_2	J_3	J_4	J_5
1	0.95	0.99	0.90	0.03	0.04	0.95	0.99	0.90	0.03	0.04	0.95	0.99	0.90	0.03	0.04
2	0.95	0.99	0.90	0.03	0.17	0.95	0.99	0.90	0.03	0.17	0.95	0.99	0.90	0.03	0.17
3	0.95	0.99	0.90	0.03	0.37	0.95	0.99	0.90	0.03	0.37	0.95	0.99	0.90	0.03	0.37
4	0.96	0.99	0.93	0.75	0.86	0.96	0.99	0.93	0.75	0.85	0.96	0.99	0.93	0.75	0.85
5	0.96	1.00	0.95	0.77	1.03	0.97	1.00	0.95	0.76	1.01	0.97	1.00	0.95	0.76	1.01
6	0.98	1.00	1.00	0.87	1.49	0.97	1.00	1.00	0.88	1.45	0.97	1.01	1.00	0.87	1.42
7	1.00	1.00	0.99	0.97	1.66	0.99	1.00	1.00	0.97	1.61	0.99	1.00	1.00	0.97	1.56

Table 12 Building B20 with μ = 10% – performance indices for the three TMD types

Set j	*TTMD*					*PTMD-60*					*PTMD-30*				
	J_1	J_2	J_3	J_4	J_5	J_1	J_2	J_3	J_4	J_5	J_1	J_2	J_3	J_4	J_5
1	0.79	0.97	0.66	0.00	0.02	0.79	0.97	0.66	0.00	0.02	0.79	0.97	0.66	0.00	0.02
2	0.79	0.97	0.66	0.00	0.06	0.79	0.97	0.66	0.00	0.06	0.79	0.97	0.66	0.00	0.06
3	0.79	0.97	0.66	0.00	0.13	0.79	0.97	0.66	0.00	0.13	0.79	0.97	0.66	0.00	0.13
4	0.81	0.98	0.76	0.34	0.33	0.81	0.98	0.76	0.34	0.33	0.81	0.98	0.76	0.34	0.33
5	0.81	0.99	0.83	0.36	0.42	0.81	0.99	0.83	0.36	0.42	0.81	0.99	0.83	0.36	0.42
6	0.86	0.99	0.96	0.54	0.75	0.86	0.99	0.96	0.54	0.75	0.86	0.99	0.96	0.54	0.75
7	0.91	1.00	0.97	0.77	0.96	0.91	0.99	0.97	0.77	0.96	0.91	0.99	0.97	0.77	0.96

Tables 7 to 12 report the conventional performance indices obtained through the multiple-stripe dynamic analyses. Each table refers to a different building and a different mass ratio, and contains in columns the five performance indices for the three TMD types, while the lines refer to increasing seismic levels. Based on these results, the following observations can be made:

- As expected, a progressive performance degradation is observed with the increase of the intensity level, as the result of structural nonlinearities and TMD mistuning. For the highest intensity, the TMD effectiveness is virtually annulled in most cases and particularly for the first three performance indices (representing peak response quantities), with the only exception of J_1 (inter-storey drift) for buildings B09 and B20 and for μ = 10%. This shows that larger mass ratios ensure the TMD a larger robustness. In several cases, the TMD appears even detrimental, providing indices larger than 1.
- For μ = 10%, results are generally scarcely dependent on the TMD type, because the large mass ratio ensures at the same time a smaller TMD stroke demand (as a result of the larger TMD damping ratio) and a larger TMD stroke capacity (as a result of the smaller TMD frequency ratio). The only exception is represented by PTMD-30 for building B03, where the premature bumping largely amplifies J_2 (accelerations) and J_3 (base shear) under the four highest intensity levels, and also J_1 under the two highest levels.
- For μ = 1%, the dependence of the performance indices on the TMD type is a little stronger, but only in terms of J_1 (inter-storey drift) and J_5 (TMD stroke). For building B03, the disproportion between the PTMD stroke capacity (approximately 0.24 m for the PTMD-60 and 0.14 m for the PTMD-30, before activation of the bumper) and the TMD stroke demand (expressed by the value of J_5 computed for the TTMD and equal to 0.52 m for the highest intensity) produces large reductions of J_5 for the PTMD-60 type and even more for the PTMD-30, and correspondingly slight reductions of J_1. The said disproportion is less evident for building B09, where reductions of J_1 and J_5 are still present but smaller, and nearly absent for building B20, where the three types substantially provide the same performance.

In order to express in monetary terms the PTMD control degradation observed above, a LCC perspective can be adopted instead of the conventional evaluation based on performance indices. By applying the approach presented in Section 3, Figure 5 exemplifies the building damage cost $C_{DS,S}$ for the three uncontrolled buildings (on the left) and for the same buildings equipped with a TTMD having μ = 10% (on the right), decomposed into damage states and storey levels. Because the cost of the 1st damage state ('1-none') is null, only six damage states are depicted for each storey level, from the 2nd one (on the left) to the 7th one (on the right).

Summing up along the building height, and extending the observation to both mass ratios and to the three TMD types, Figure 6 is obtained, where the total LCC $C = C_{DS,S} + C_T$ is shown, normalised to the total uncontrolled LCC C_{unc}. Similar to Figure 5, $C_{DS,S} / C_{unc}$ is decomposed into seven damage states, but a brown rectangle is now added to represent the normalised TMD cost C_T / C_{unc}, computed according to Section 3.2.2. The white rectangle with dashed contour represents the normalised cost savings C_{save}/C_{unc}, i.e., the TMD cost-effectiveness *CE*.

Figure 5 Building damage cost for the three uncontrolled buildings (left) and for the buildings equipped with an optimal TTMD having μ = 10% (right), decomposed among storey levels and damage states (see online version for colours)

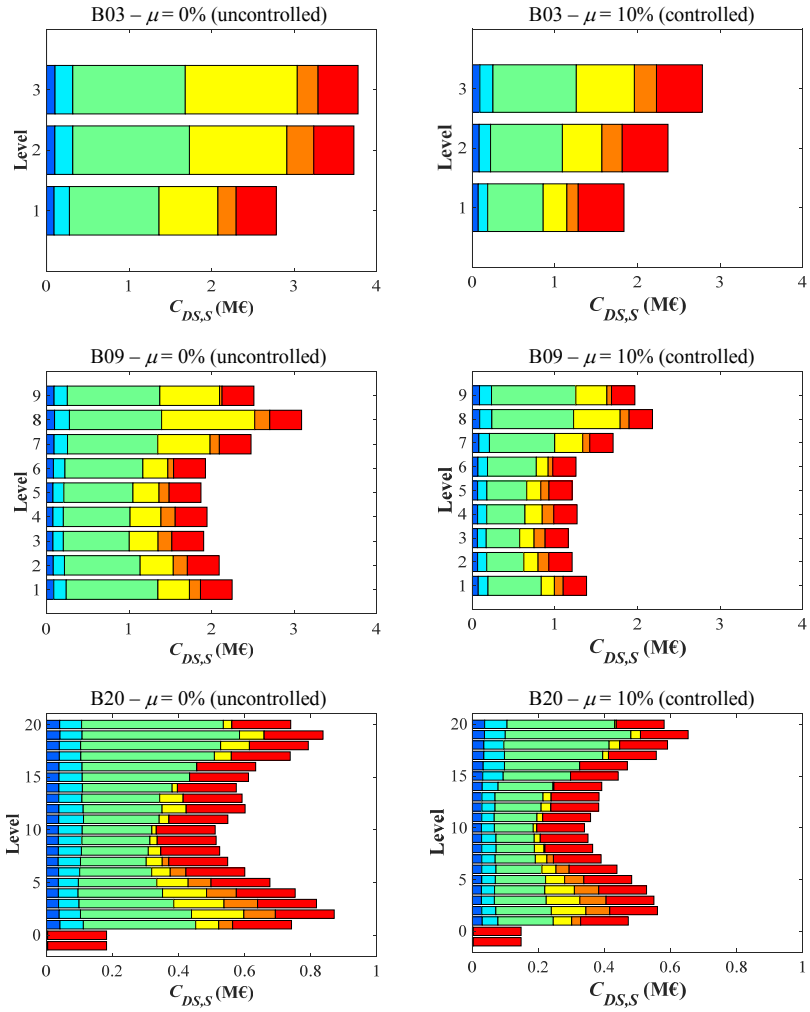

Note: Legend for the damage states: 1 (null); 2 (blue); 3 (azure); 4 (green); 5 (yellow); 6 (orange); 7 (red).

Results are finally summarised in Tables 13 and 14. Table 13 reports the normalised building LCC $C_{DS,S}$ / C_{unc} and the normalised TMD LCC C_T / C_{unc}, for all the examined design scenarios. While $C_{DS,S}$ / C_{unc}, which depends on the TMD efficacy, is different for the three TMD types (lines 1 to 3), the TMD cost, which substantially depends only on the absorber mass, is unique for the three types (line 4). Table 14 reports the TMD cost-effectiveness $CE = 1 - C / C_{unc}$ for all considered design scenarios.

Table 13 Building LCC ($C_{DS,S}$) and TMD LCC (C_T) normalised to the uncontrolled LCC (C_{unc}) for the three TMD types

LCC term	*TMD type*	*B03*		*B09*		*B20*	
		μ = 1%	*μ = 10%*	*μ = 1%*	*μ = 10%*	*μ = 1%*	*μ = 10%*
$C_{DS,S}$ / C_{unc}	TTMD	0.856	0.680	0.901	0.665	0.925	0.705
	PTMD-60	0.883	0.684	0.903	0.668	0.923	0.706
	PTMD-30	0.907	0.715	0.917	0.668	0.923	0.706
C_T / C_{unc}	All	0.007	0.073	0.011	0.113	0.021	0.206

Table 14 Cost-effectiveness $CE = 1 - C / C_{unc}$ for the three TMD types

TMD type	*B03*		*B09*		*B20*	
	μ = 1%	*μ = 10%*	*μ = 1%*	*μ = 10%*	*μ = 1%*	*μ = 10%*
TTMD	0.137	0.247	0.087	0.222	0.055	0.090
PTMD-60	0.109	0.243	0.085	0.219	0.057	0.089
PTMD-30	0.086	0.212	0.071	0.219	0.056	0.089

Figure 6 Normalised total LCC C / C_{UNC}, reported for the two mass ratios (μ = 1% on the left, μ = 10% on the right), the three buildings and the four control configurations, decomposed into damage state costs and TMD cost (a) μ = 1% (b) μ = 10% (see online version for colours)

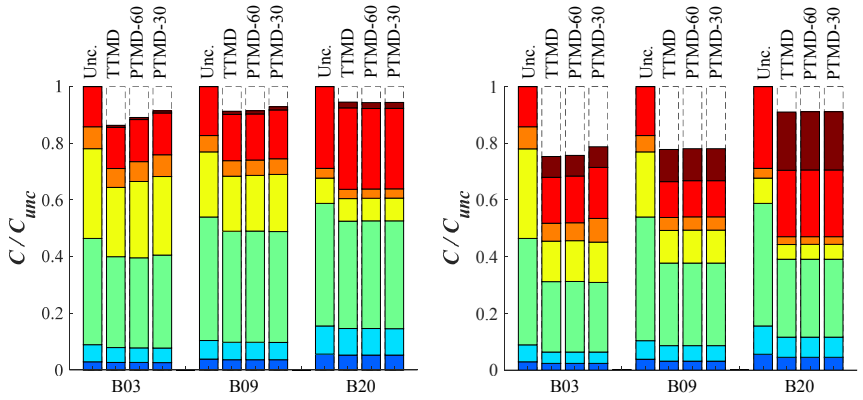

Notes: Legend for the damage states: 1 (null); 2 (blue); 3 (azure); 4 (green); 5 (yellow); 6 (orange); 7 (red). Legend for the TMD cost: brown; white rectangles: TMD cost-effectiveness.

The most significant results in Figures 5 to 6 and Tables 13 to 14 can be commented as follows:

- The uncontrolled building damage cost $C_{DS,S}$ equals 10.28 M€, 20.06 M€ and 13.60 M€, respectively for buildings B03, B09 and B20, corresponding to an average cost per unit area equal to, respectively, 1,707 €/m^2, 1,066 €/m^2 and 609 €/m^2 (Figure 5). These different unit costs reflect the differences among the inter-storey drift ratios resulting from the analyses, which in fact decrease from B03 to B20. In

monetary terms, B03 is the more seismically vulnerable of the three buildings, followed by B09 and finally by B20.

- In the uncontrolled cases, the damage state which most contributes to $C_{DS,S}$ is always the 4th one ('4-moderate'), followed, for B03 and B09, by the 5th one ('5-heavy') and then by the 7th one ('7-destroyed'), and for B20 directly by the 7th one (Figures 5 and 6). In general, the intermediate damage states (mainly 4 and 5) are those which experience the most expensive combination of occurrence probability and damage severity.
- The intermediate damage states are also those where the TMD effectiveness achieves its best, because building damage costs are maximum and structural nonlinearities are not yet large enough to impair the TMD performance (Tables 7 to 12). As a result, a significant reduction of $C_{DS,S}$ can be provided by the TMD even when its efficacy is heavily degraded under the most severe seismic levels (Figure 6). The larger the TMD mass ratio, the larger the reduction. Looking for example at a TTMD with a 1% mass ratio, $C_{DS,S}$ is reduced to 85.6%, 90.1% and 92.5%, respectively for buildings B03, B09 and B20 (Table 13). These percentages further reduce to 68.0%, 66.5% and 70.5% if a 10% mass ratio is assumed.
- On the other hand, the larger the TMD mass ratio, the larger the retrofitting cost C_T (Table 13). Independently from the TMD type, for $\mu = 1\%$ C_T / C_{unc} equals 7.3%, 11.3% and 20.6%, respectively for buildings B03, B09 and B20. For $\mu = 10\%$, C_T / C_{unc} increases approximately 10 times, to respectively 7.3%, 11.3% and 20.6%. Noticeably, these percentages decrease from B03 to B20, together with the building damage cost per unit area, indicating that the TMD is more convenient when the expected seismic damage costs are larger. Consequently, as the mass ratio increases and the seismic vulnerability decreases, the TMD investment cost may represent a large percentage of C_{unc}, making progressively less profitable the retrofitting intervention.
- Because the three TMD types exhibit a different performance under large seismic loads (Tables 7 to 12), their corresponding lifecycle efficacy is also different, as clearly visible in Figure 6. This appears both in Table 13, where $C_{DS,S}$ and C_T are kept separate, and in Table 14, where $C_{DS,S}$ and C_T are combined in the cost-effectiveness *CE*. Both tables highlight the differences among the proposed TMD types in a LCC perspective, in a much more concise and objective manner than the conventional performance indices may permit.
- Table 14, in particular, shows that the three options are nearly equivalent for building B20 (with *CE* around 5.6% for $\mu = 1\%$ and around 8.9% for $\mu = 10\%$) and also for B09 only if $\mu = 10\%$ (with *CE* around 22.0%). For building B09 and $\mu = 1\%$, instead, *CE* is nearly the same for the TTMD and the PTMD-60 options (around 8.6%) while for the PTMD-30 type is reduced to 7.1%. For building B03, the PTMD performance reduction is even more evident: if $\mu = 10\%$, CE is still similar for the TTMD and the PTMD-60 (around 24.5%) but reduces to 21.2% for the PTMD-30; if $\mu = 1\%$, *CE* is 13.7% for the TTMD, 10.9% for the PTMD-60 and only 8.6% for the PTMD-30.
- These results show that, with respect to an ideal translational TMD, a pendulum TMD may experience a non-negligible cost-effectiveness degradation, its performance depending on its stroke capacity, i.e., on the intrinsic constraint

expressed by its curved trajectory and by the additional fail-safe bumper. In all the examined case studies, whenever for a PTMD a significant reduction of the stroke index J_5 is observed with respect to the corresponding TTMD, a non-negligible degradation of the PTMD cost-effectiveness is reported. A reliable mechanical nonlinear model and a LCC analysis approach are necessary to fully detect the extent of such degradation.

7 Conclusions

The main conclusions of the present work can be summarised as follows:

1 For the examined benchmark case studies, representative of typical existing steel buildings located in high seismicity regions, the adopted LCC evaluation methodology, applied here for the first time to both linear TTMDs and nonlinear PTMDs, shows that both types are a cost-effective seismic retrofitting strategy. Despite the poor control performance that both types exhibit against the most severe hazards, they still prove a profitable investment for reducing the economic consequences of future earthquakes.

2 Because of the geometric and mechanical nonlinearities inherent in their pendular arrangement and in the associated fail-safe bumper, PTMDs may undergo a performance degradation with respect to TTMDs, which increases with the seismic intensity and is larger for short-period structures and small mass ratios. Reliable mechanical nonlinear models and comprehensive LCC approaches are necessary to rationally and concisely measure this degradation, directly expressing it in monetary terms.

3 In the proposed examples, the PTMD cost-effectiveness reduction results non-negligible for the low and medium-rise buildings if small mass ratios are used and if the bumper is prematurely activated. In the worst case, corresponding to a bumping clearance of 30°, cost-effectiveness reduction equals 37%. Better results are obtained with a 60° clearance, with reductions never greater than 20%. In general, whenever for a PTMD the analyses report significant stroke reductions with respect to those obtained with a TTMD, significant reductions of the PTMD cost-effectiveness are to be expected.

4 On the other hand, the adoption of large mass ratios and large bumping angles ensures the TTMD and the PTMD a nearly identical lifecycle performance and the maximum cost-effectiveness, practically outlining the best strategy for a seismically-oriented TMD design.

References

FEMA-273 (1997) *NEHRP Guidelines for Seismic Rehabilitation of Buildings*, Federal Emergency Management Agency, Washington, DC.

Fragiadakis, M. and Lagaros, N.D. (2011) 'An overview to structural seismic design optimisation frameworks', *Computers and Structures*, Vol. 89, Nos. 11–12, pp.1155–1165.

Ghobarah, A., Abou-Elfath, H. and Biddah, A. (1999) 'Response-based damage assessment of structures', *Earthquake Engineering and Structural Dynamics*, Vol. 28, No. 1, pp.79–104.

Gupta, A. and Krawinkler, H. (1999) *Seismic Demands for Performance Evaluation of Steel Moment Resisting Frame Structures*, Report No. 132, June, The John A. BLume Earthquake Engineering Center, Stanford University, Stanford, CA.

Hahm, D., Ok, S-Y., Park, W., Koh, H-M. and Park, K-S. (2013) 'Cost-effectiveness evaluation of an MR damper system based on a life-cycle cost concept', *KSCE Journal of Civil Engineering*, Vol. 17, No. 1, pp.145–154.

Huang, M.F., Tse, K.T., Chan, C.M., Lou, W.J. (2011) 'Integrated structural optimization and vibration control for improving wind-induced dynamic performance of tall buildings', *Int. J. Struct. Stab. Dyn.*, Vol. 11, No. 6, pp.1139–1161.

Kappos, A.J. and Dimitrakopoulos, E.G. (2008) 'Feasibility of pre-earthquake strengthening of buildings based on cost-benefit and life-cycle cost analysis, with the aid of fragility curves', *Natural Hazards*, Vol. 45, No. 1, pp.33–54.

Lee, C.S., Goda, K. and Hong, H.P. (2012) 'Effectiveness of using tuned-mass dampers in reducing seismic risk', *Structural and Infrastructural Engineering*, Vol. 8, No. 2, pp.141–156.

Lukkunaprasit, P. and Wanitkorkul, A. (2001) 'Inelastic buildings with tuned mass dampers under moderate ground motions from distant earthquakes', *Earthquake Engineering and Structural Dynamics*, Vol. 30, No. 4, pp.537–551.

Matta, E. (2017) 'Lifecycle cost optimization of tuned mass dampers for the seismic improvement of inelastic structures', *Earthquake Engineering and Structural Dynamics*, Vol. 47, No. 3, pp.714–737.

Matta, E. and De Stefano, A. (2009) 'Seismic performance of pendulum and translational roof-garden TMDs', *Mechanical Systems and Signal Processing*, Vol. 23, No. 3, pp.908–921.

Mitropoulou, C.C., Lagaros, N.D. and Papadrakakis, M. (2011) 'Life-cycle cost assessment of optimally designed reinforced concrete buildings under seismic actions', *Reliability Engineering and System Safety*, Vol. 96, No. 10, pp.1311–1331.

Ohtori, Y., Christenson, R.E., Spencer Jr., B.F. and Dyke, S.J. (2004) 'Benchmark control problems for seismically excited nonlinear buildings', *Journal of Engineering Mechanics*, Vol. 130, No. 4, pp.366–385.

Pinkaew, T., Lukkunaprasit, P. and Chatupote, P. (2003) 'Seismic effectiveness of tuned mass dampers for damage reduction of structures', *Engineering Structures*, Vol. 25, No. 1, pp.39–46.

Ruiz, R., Taflanidis, A.A., Lopez-Garcia, D. and Vetter, C.R. (2016) 'Life-cycle based design of mass dampers for the Chilean region and its application for the evaluation of the effectiveness of tuned liquid dampers with floating roof', *Bulleting of Earthquake Engineering*, Vol. 14, No. 6, pp.943–970.

Sadek, F., Mohraz, B., Taylor, A.W. and Chung, R.M. (1997) 'A method of estimating the parameters of tuned mass dampers for seismic applications', *Earthquake Engineering and Structural Dynamics*, Vol. 26, No. 3, pp.617–635.

Sanchez-Silva, M. and Rackwitz, R. (2004) 'Socioeconomic implications of life quality index in design of optimum structures to withstand earthquakes', *Journal of Structural Engineering*, Vol. 130, No. 6, pp.969–977.

Shin, H. and Singh, M.P. (2014) 'Minimum failure cost-based energy dissipation system designs for buildings in three seismic regions – Part I: elements of failure cost analysis', *Engineering*

Structures, Vol. 74, pp.266–274 [online] https://www.sciencedirect.com/science/article/pii/S0141029614003289.

Somerville, P., Smith, N., Punyamurthula, S. and Sun, J. (1997) *Development of Ground Motion Time Histories for Phase 2 of the FEMA/SAC Steel Project*, SAC Background Document, Report No. SAC/BD-97/04.

Soto-Brito, R. and Ruiz, S.E. (1999) 'Influence of ground motion intensity on the effectiveness of tuned mass dampers', *Earthquake Engineering and Structural Dynamics*, Vol. 28, No. 11, pp.1255–1271.

Spencer Jr., B.F. and Nagarajaiah, S. (2003) 'State of the art of structural control', *Journal of Structural Engineering*, Vol. 129, No. 7, pp.845–856.

Taflanidis, A.A. and Beck, J.L. (2009) 'Life-cycle cost optimal design of passive dissipative devices', *Structural Safety*, Vol. 31, No. 6, pp.508–522.

Taflanidis, A.A., Angelides, D.C. and Scruggs, J.T. (2009) 'Simulation-based robust design of mass dampers for response mitigation of tension leg platforms', *Engineering Structures*, Vol. 31, No. 4, pp.847–857.

Villaverde, R. and Koyama, L.A. (1993) 'Damped resonant appendages to increase inherent damping in buildings', *Earthquake Engineering and Structural Dynamics*, Vol. 22, No. 6, pp.491–507.

Wang, D., Tse, T.K.T., Zhou, Y. and Li, Q. (2015) 'Structural performance and cost analysis of wind-induced vibration control schemes for a real super-tall building', *Structural and Infrastructural Engineering*, Vol. 11, No. 8, pp.990–1011.

Wen, Y.K. and Kang, Y.J. (2001) 'Minimum building life-cycle cost design criteria. II: applications', *Journal of Structural Engineering*, Vol. 127, No. 3, pp.338–346.

Wong, K.K.F. (2008) 'Seismic energy dissipation of inelastic structures with tuned mass dampers', *Journal of Engineering Mechanics*, Vol. 134, No. 2, pp.163–172.

Nomenclature

A_i	Absolute horizontal acceleration at the i^{th} storey
$\mathbf{C}$	Structural damping matrix
C	Total controllable lifecycle cost
CE	TMD cost-effectiveness
$C_{DS,S}$	Building lifecycle damage state cost
$C_{DS,T}$	TMD lifecycle damage state cost
$C_{IN,S}$	Building initial cost
$C_{IN,T}$	TMD initial cost
C_{save}	Lifecycle cost savings
C_T	TMD lifecycle cost
C_{TOT}	Total lifecycle cost
C_{unc}	Uncontrolled building lifecycle damage state cost
C^i_{con}	Loss of contents cost for the i^{th} damage state
C^i_{dam}	Damage repair cost for the i^{th} damage state
C^i_{fat}	Human fatality cost for the i^{th} damage state
C^i_{inc}	Loss of income cost for the i^{th} damage state

C_{inj}^{i}	Injury cost for the i^{th} damage state
C_{ren}^{i}	Loss of rental cost for the i^{th} damage state
c_T	TMD damping coefficient
c_U	TMD cost per unit mass
$\mathbf{f}_{p-\Delta}$	Vector of P-delta forces
$\mathbf{f}_r$	Vector of lateral restoring forces
g	Gravity acceleration
J_1	Controlled-to-uncontrolled ratio of the maximum peak inter-storey drift
J_2	Controlled-to-uncontrolled ratio of the maximum peak absolute acceleration
J_3	Controlled-to-uncontrolled ratio of the peak base shear force
J_4	Controlled-to-uncontrolled ratio of the total energy dissipated in the inelastic hinges
J_5	Mean value of the peak TMD horizontal stroke
$\mathbf{K}$	Total structural stiffness matrix
$\mathbf{K}_e$	First-order elastic structural stiffness matrix
$\mathbf{K}_{P-\Delta}$	Geometric structural stiffness matrix
k_T	TMD stiffness
k_φ	Bumper rotational stiffness
$\mathbf{M}$	Structural mass matrix
m_S	total structural mass
m_T	TMD mass
N_D	Number of damage states
N_L	Number of intensity levels
N_R	Number of two-component records
N_S	Number of storey levels
$\mathbf{P}$	P-delta cumulative gravity load matrix
p_T	Structure-TMD interaction force
$P_{e/\tau}^{i}$	Probability of exceedance of the i^{th} intensity level in the time period τ
P_o^i	Occurrence probability of the i^{th} damage state
R	Pendulum length
r	TMD-to-structure frequency ratio
$\mathbf{T}$	Rotation matrix
t	Lifetime period
t_a	Actualised lifetime period
$\mathbf{t}_{\underline{g}}$	Topological vector for the ground acceleration
$\mathbf{t}_{\underline{p}}$	Topological vector for the interaction force
$\mathbf{u}$	Vector of horizontal structural displacements relative to the ground
$\dot{\mathbf{u}}$	Vector of horizontal structural velocities relative to the ground
$\ddot{u}_g$	Ground acceleration input
u_T	TMD horizontal displacement relative to the top storey (stroke)

$\dot{u}_T$	TMD horizontal velocity relative to the top storey
V_b	Structure base shear force
ς_S	Damping ratio of the structural target mode
ς_T	Damping ratio of the TMD
$\boldsymbol{\theta}$	Vector of inter-storey drift ratios
λ	Momentary discount rate
μ	TMD-to-structure mass ratio
ν	Mean occurrence frequency of significant earthquakes
ρ	Bumper-to-pendulum stiffness ratio
τ	Time period
φ	PTMD angular displacement
$\dot{\varphi}$	PTMD angular velocity
$\ddot{\varphi}$	PTMD angular acceleration
$\varphi_{\max}$	Bumper angular clearance
φ_e^i	Mean exceedance frequency of the i^{th} damage state
φ_o^i	Mean occurrence frequency of the i^{th} damage state
χ	Tangential force transmitted by the PTMD to the bumper
ω_S	Circular frequency of the structural target mode
ω_T	TMD circular frequency
ω_φ	Bumper circular frequency